Far-infrared dichroic bandpass filters

D. D. Nolte, A. E. Lange, and P. L. Richards

Filters which serve as dichroic beam dividers are useful for certain types of far-infrared photometer. We have used inductive cross metal mesh as reflective coatings on solid dielectric Fabry-Perot etalons to produce dichroic filters with quality factors in the range $3 < Q < 10$. These filters reflect strongly at frequencies below the bandpass and retain their well-defined bandpass at angles of incidence as large as 45°. They have been used to make an efficient far-infrared dichroic photometer with six frequency bands between 10 and 100 cm^{-1}.

I. Introduction

Certain applications of far-infrared photometry to plasma diagnostics and astrophysics require measurements of transient phenomena in one region of space simultaneously at several frequencies. Several technologies exist which permit such dichroic photometers to be made. Diffraction gratings are efficient dichroic elements if the required frequency bands are narrow and the wavelength range not too large. Reststrahlen reflection filters provide efficient dichroic band separation at frequencies where they are available.

We were interested in constructing a far-infrared dichroic photometer for a rocket measurement of astrophysical backgrounds between 10 and 100 cm^{-1}. For this experiment it was necessary to separate the frequency range into six nearly contiguous bands. Since neither of the above technologies was appropriate for this application, we developed a new approach to the dichroic problem.

Fabry-Perot (F.P.) etalons made from capacitive or inductive metal mesh are well-known bandpass filters at far-infrared frequencies. Although these etalons tend to reflect strongly at frequencies below the transmittance band, their usefulness as dichroic filters is limited by the fact that their bandpass characteristics degrade rapidly as the angle of incidence increases from zero. It is a matter of great convenience in a far-infrared optical system to have large angular separations between dichroic channels.

Our approach was to use F.P. etalons made from the inductive cross metallic mesh discussed by Ulrich.[1,2] The use of such etalons as bandpass filters has been discussed by Davis,[3] Tomaselli *et al.*,[4] Chase *et al.*[5] and Cunningham.[6] Several workers have minimized the amount of dielectric in the etalon to maximize filter efficiency. We use solid dielectric etalons at some cost in efficiency to minimize internal angles when the etalons are used at large angles of incidence.

In this paper we discuss the theory of etalons made from inductive cross mesh deposited on both sides of dielectric substrates. We show that the phase shift on reflection from an inductive cross mesh can be used to superimpose different orders of interference and to control the bandpass characteristics in a useful way. Finally, we present practical design data and measured performance for dichroic bandpass filters used with the angle of incidence equal to 45°.

II. Model

Our filters can be modeled as F.P. etalons with frequency-dependent reflectivity and frequency-dependent phase shift on reflection at the mesh. This frequency dependence is provided by the resonant properties characteristic of the inductive cross metallic mesh. In the more conventional inductive or capacitive mesh[7,8] the mesh resonance is close to the frequency at which diffraction effects begin. In the inductive cross mesh the mesh resonance occurs at frequencies far enough below the onset of diffration that it can be used to tailor the properties of the filter. Our analysis follows the approach used by Ulrich[2] to analyze etalons made from inductive mesh operated far from diffraction. The condition for Fabry-Perot transmittance maxima at normal incidence is

$$\frac{2\pi nt}{\lambda} + \phi = N\pi \qquad N = 0,1,2,\ldots, \tag{1}$$

where t is the thickness of the substrate, n is the index

The authors are with University of California, Berkeley, California 94720.

Received 28 November 1984.
0003-6935/85/101541-05$02.00/0.

of refraction of the substrate, and ϕ is the phase shift for a single internal reflection. For the case of an etalon made from a bare dielectric slab in a vacuum, $\phi = 0$, and the F.P. peaks are evenly spaced in frequency. If the phase shift for internal reflection is a function of frequency, however, the F.P. peaks will no longer be equally spaced but will occur at frequencies which must be determined from the combined contributions to the phase shift from the path difference and the internal reflection.

A well-known type of microwave waveguide bandpass filter makes use of this phenomenon.[9] In a quarter-wavelength filter, two resonant structures are separated by a waveguide which is one-quarter of a guide wavelength long at the resonant frequency. The phase shift on reflection from the resonant structure jumps from $-\pi/2$ below resonance to $\pi/2$ above resonance. In the approximation that the jump in phase is discontinuous, the $N = 0$ and $N = 1$ orders of the etalon both occur at the frequency of the resonant structures. These coincident orders form the single passband of the filter. Other orders are less important because they occur away from the resonant frequency of the structures and thus have very high finesse.

A. Inductive Cross Mesh

Our filters are made for far-infrared applications by using inductive cross mesh (ICM) in place of the microwave resonant structures. The ICM pattern has three parameters: the grid spacing g, the inductive element width $2a$, and the capacitive element width $2b$, as are shown in Fig. 1. Several approaches to the analysis of electromagnetic scattering from metallic mesh are reviewed by Durschlag and DeTemple.[10] Following the approach of Anderson,[11] the results of Marcuvitz[12] can be used to obtain expressions for the effective capacitance C and inductance L of the mesh. These quantities are then used in an equivalent parallel LC resonant circuit to compute the lumped-circuit equivalent reactance X_g of the mesh. Assuming that both a and b are small compared with g, the expression for X_g is

$$X_g = \left(\frac{L}{C}\right)^{1/2} \frac{\omega\omega_0}{(\omega_0^2 - \omega^2)}, \tag{2}$$

where

$$L/C \cong \frac{b \ln(g/\pi a)}{2(g - 2b - 2a)\ln(g/\pi b)}, \tag{3}$$

and the resonant frequency is

$$\omega_0 = (LC)^{-1/2} \simeq \pi[2b(g - 2b - 2a)\ln(g/\pi a)\ln(g/\pi b)]^{-1/2}. \tag{4}$$

The expression for L/C agrees well with our experiments, but the expression for ω_0 gives values which are too large by approximately a factor of 2. This discrepancy in ω_0 is due to the deviation of the actual values of L and C from the theoretical expressions as the angular frequency approaches the value $2\pi/ng$ at which the diffraction begins. In this work $\omega_0 \simeq 0.8(2\pi/ng)$. Diffraction corrections to the frequency ω_0 which depend on the product LC are large, while corrections to L/C are small.

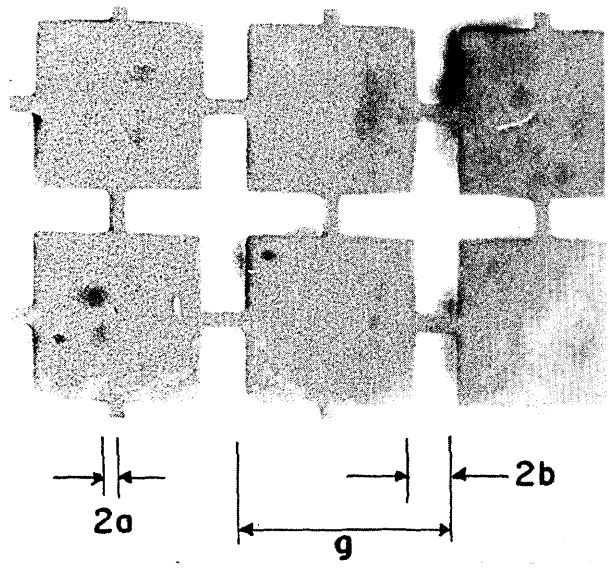

Fig. 1. Photograph of aluminum inductive cross mesh on Mylar substrate. The grid on the reverse side is out of focus and appears as a shadow. The definitions of the mesh parameters a, b, and g are shown. In this case, $g = 164$ μm.

B. Influence of the Dielectric Substrate

When a resonant mesh is placed on a dielectric substrate, the behavior of the mesh is affected in several ways. Most important for the fabrication of dichroic beam dividers, a large index of refraction for the substrate allows good filter performance at large angles of incidence because of the reduction in internal angles. Also, the effective capacitance of the mesh on the dielectric is greater than its free space value. Timusk and Richards[13] proposed the relation

$$C_n = \tfrac{1}{2}(n^2 + 1)C_{\text{free}}, \tag{5}$$

which assumes that the increase is equivalent to half-filling a capacitor with dielectric. This conjecture is supported by detailed calculations due to Compton,[14] although there has been considerable debate in the literature.[10,15] This increase in capacitance decreases ω_0. The index of refraction of the substrate also appears in the expression $2\pi/ng$ for the frequency at which diffraction becomes important and in the expression for the phase shift experienced on internal reflection.

The amplitude reflection coefficient r and the phase shift ϕ on internal reflection from the dielectric–mesh–air interface can be calculated in terms of the equivalent circuit reactance X_g for a lossless mesh by matching boundary conditions,

$$r = \frac{X_g^2(n^2 - 1) - 1 - 2iX_g n}{X_g^2(n + 1)^2 + 1}, \tag{6}$$

$$\phi = \tan^{-1}\left|\frac{-2X_g n}{X_g^2(n^2 - 1) - 1}\right| \mp \pi. \tag{7}$$

When mesh are deposited on both sides of the substrate, the standard results for a F.P. etalon are

$$\frac{I_t}{I_i} = \left(1 - \frac{A}{1 - R}\right)^2 \cdot \frac{1}{1 + F\sin\delta/2}, \tag{8}$$

where

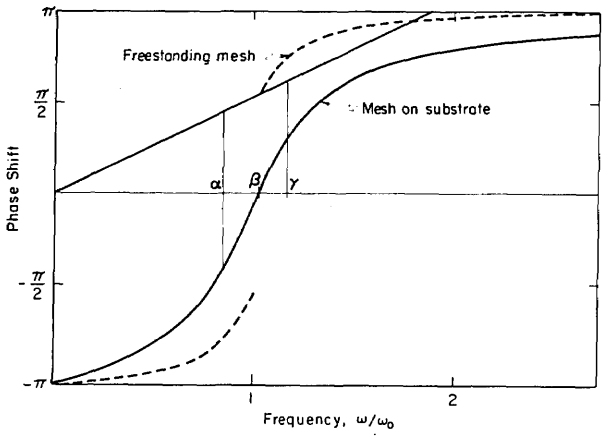

Fig. 2. Plot of phase shift computed for a single internal reflection from a resonant inductive cross mesh. The dashed curve for the freestanding mesh has a phase discontinuity at resonance. The solid phase curve for a mesh on a dielectric substrate is continuous through the resonance. The contribution to the phase shift from a single transmittance through a substrate of thickness $\lambda/4n$ is also plotted as a diagonal straight line. For the freestanding mesh, the $N = 0$ and $N = 1$ orders of the etalon occur at frequency β. For the mesh on a dielectric substrate, the order $N = 0$ occurs at frequency α where the reflection and path difference phase shifts add to zero. The order $N = 1$ occurs at frequency γ where the two phase shifts add to π.

$$F = \frac{4R}{(1-R)^2}, \qquad \delta = \frac{4\pi}{\lambda} nt\cos\theta' + 2\phi. \tag{9}$$

and θ' is the angle of incidence in the medium. Here $R = |r|^2$ and A are the power reflectance and absorptance coefficients for a single mesh.

To illustrate the importance of these relationships for our filters, we have shown in Fig. 2 the phase shift ϕ for a single internal reflection given by Eq. (7). Equation (7) is plotted for $L/C = 0.028$ for a freestanding mesh and also for a mesh on a dielectric substrate with $n = 1.7$. We have also shown the phase shift $2\pi nt/\lambda$ which arises from a single traversal of an etalon of thickness $nt = \lambda/4$.

For the case of the freestanding mesh, there is a jump of π in the phase shift at the resonant frequency of the mesh. For this reason, both the $N = 0$ and the $N = 1$ orders occur at the resonant frequency marked β. For the mesh on the dielectric, the phase function is continuous and the order $N = 0$ occurs at the frequency marked α and the order $N = 1$ occurs at the frequency marked γ. The bandwidth of the resulting filter is strongly influenced by the separation of these two transmittance peaks. This separation is determined by the slope of the curve of reflection phase shift vs frequency, and hence by L/C for the mesh and also by the index n of the substrate.

Changes in the thickness t of the etalon change the slope of the path-difference contribution to the phase shift. This leads to a change in the frequency of the passband which is significantly less than would be expected for an etalon with nonresonant mesh. As a consequence, the requirements for flatness and parallelism are relaxed significantly compared with etalons with nonresonant reflectors. This could be of considerable importance in producing high finesse etalons with freestanding mesh.

Diffraction effects at frequencies above $2\pi/ng$ provide significant attenuation on the high frequency side of the bandpass. The amount of energy diffracted out of the beam depends on the optics of the detection system.

III. Construction of Filters

The peak transmittance of our filters depends strongly on the quality of the aluminum films which were 0.12 μm thick. When Mylar substrates were used, the evaporation rate was kept below 5 Å/sec to avoid heating the Mylar and causing it to curl. Care was taken to insure that the film quality was the same on both sides of the substrate. We used the facilities of the U.C. Berkeley Microfabrication Laboratory to pattern the Al films. The masks for lower frequencies were produced directly on a computerized mask generator. A step-and-repeat camera was used to obtain masks with sufficient area for the 32- and 80-cm^{-1} filters. Conventional contact printing and Hg arc lamp exposure were used with Shipley[16] 1350-J positive photoresist. The quality of the mesh pattern affects both the peak transmittance and the bandwidth of the filter. Care was required during contact printing to insure that the mask and Mylar were flat. Overdevelopment of the photoresist which could produce rounded corners of the mesh was avoided. The aluminum was etched at 50°C using Transene[17] Type-A aluminum etch until the unprotected aluminum had visibly cleared. An additional 6 sec of etch was used to insure that no optically thin film remained. An example of the resulting mesh pattern is shown in Fig. 1.

IV. Filter Evaluation

Filter measurements were made using a Michelson Fourier spectrometer with $f/2$ optics. The detector was a helium-cooled bolometer.[18] The filters could be tested at either room temperature or immersed in superfluid helium. Some improvement in transmittance occurred for cold filters, presumably due to reduction in the ohmic and/or dielectric loss.

High purity Si with resistivity near 500 Ω cm has negligible absorption and a large index $n = 3.4$. It can easily be etched into parallel sided sheets as thin as 75 μm, which correspond to filter transmittance peaks near 10 cm^{-1}. Transmittance measurements of an etalon which had ICM with $g = 125$, $a = 0.05$, and $b = 0.13$ μm on both sides of a 75-μm Si substrate gave a well-defined filter bandpass with a 10% bandwidth and a peak transmittance of 0.65. The performance of this filter was insensitive to angle up to 45° incidence. The extension of this technology to higher frequencies is limited because it becomes difficult to fabricate the required Si substrates.

Since our application required higher frequencies and broader bandwidths, we used Mylar polyester substrates with $n = 1.7$. The parameters of four filters made on Mylar substrates are given in Table I.

Table I. Parameters for Dichroic Bandpass Filters on Mylar Substrates with $n = 1.7$ [a]

ν (cm^{-1})	t (μm)	tn/λ_0	g (μm)
10	175	0.30	375
15	100	0.26	250
23	75	0.30	164
32	50	0.28	118

[a] For each case $a = 0.05g$ and $b = 0.09g$; transmittance curves for these filters are given in Fig. 4.

Figure 3 shows the transmittance of a typical bandpass filter measured both at normal incidence and at 45° incidence. Some changes in the passband are observed, largely due to small changes in the frequencies of the resonances of order $N = 0$, 1, and 2.

Figure 4 shows individual transmittance curves measured at 45° incidence for four filters whose parameters are given in Table I. Reflectance measurements were also made at 45° incidence for several filters. The sum of reflectance and transmittance is >95° for the frequency region $\omega < 0.7\omega_0$, which is important for dichroic applications, and approaches 50% at high frequencies.

With proper selection of parameters, calculations using the theory outlined above gave transmittance curves that were in semiquantitative agreement with the measurements at frequencies below the diffraction limit. We found that calculations are very useful in guiding the selection of experimental parameters.

Several general trends can be observed in our data. The bandwidth and the peak transmittance both increase with increasing b. The bandwidth result is easily understood in terms of Eq. (3) which describes the mesh resonance. Low-Q filters tend to have high transmittance peaks because of the reduced influence of absorption. As b increases, the amount of high frequency leakage increases. This can be understood in terms of the ray-optics limit since the area free of metal increases with the increasing b.

The behavior of the filter response cannot be predicted quantitatively for frequencies in the diffraction region above $2\pi/ng$. In the absence of diffraction there should be high-order F.P. transmittance peaks. With diffraction, these transmittance peaks are diminished dramatically due to the scattering of energy into large angles. This effect can assist in providing good rejection at high frequencies.

V. Conclusions

We have found that the use of resonant ICM in F.P. etalons yields additional experimental parameters which can be selected to produce useful infrared dichroic filters. These filters have been used in a multichannel far-infrared photometer with six frequency channels between 10 and 100 cm^{-1}. The dichroic beam splitters are arranged so that the beam entering the instrument is incident on each at 45°, in order of decreasing frequency. The measured response of the four low frequency channels of this photometer is shown in Fig. 5. These measurements were made with a room temperature spectrometer and bolometric detectors.[18]

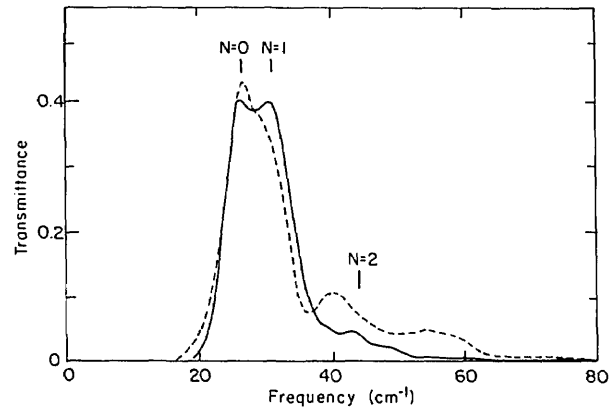

Fig. 3. Transmittance of an inductive cross mesh bandpass filter on a Mylar substrate at 1.3 K for 45° incidence (dashed line), and normal incidence (solid line). The orders of the Fabry-Perot etalon are labeled for the case of normal incidence. The parameters for this filter are $t = 75$ μm, $g = 118$ μm, $a = 0.05g$, and $b = 0.061g$.

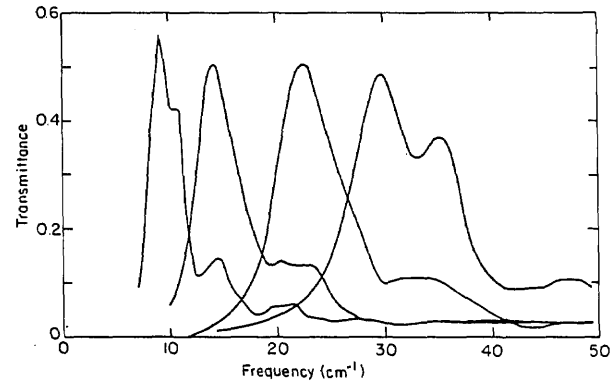

Fig. 4. Transmittance of individual ICM filters on Mylar at 1.3 K for 45° incidence. The parameters for these filters are given in Table I.

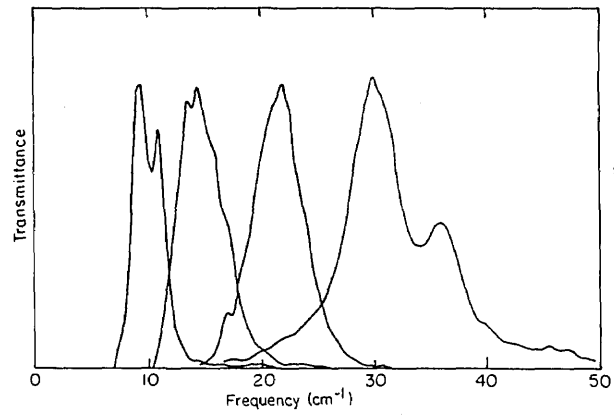

Fig. 5. Response of four channels of a dichroic photometer using the filters described in Table I plus additional low and high pass filters in each channel. The peak response has been normalized to the same value for each channel.

When comparisons are made to the transmittances of individually measured mesh etalons shown in Fig. 4, some extra structure is seen that comes from additional low and high pass filters in each channel. It is also seen

that the cut-on of one filter reduces the second-order response of the next lower frequency filter. In the complete instrument this effect will also be used to improve the shape of the 30-cm^{-1} band. The detailed design and performance of this photometer will be published elsewhere.[19]

We are very grateful to Kim Chan of the U.C. Berkeley Microfabrication Laboratory for invaluable help in producing the ICM. This work was supported by the Director, Office of Energy Research, Office of Basic Energy Sciences, Materials Sciences Division of the U.S. Department of Energy under contract DE-AC03-76SF00098.

References

1. R. Ulrich, "Interference Filters for the Far Infrared," Appl. Opt. **7,** 1987 (1968).
2. R. Ulrich, K. F. Renk, and L. Genzel, "Tunable Submillimeter Interferometers of the Fabry-Perot Type," IEEE Trans. Microwave Theory Tech. **MTT-11,** 363 (1963).
3. J. E. Davis, "Bandpass Interference Filters for Very Far IR Astronomy," Infrared Phys. **20,** 287 (1980).
4. V. P. Tomaselli, D. C. Edewaard, P. Gillan, and K. D. Moller, "Far-Infrared Bandpass Filters from Cross-Shaped Grids," Appl. Opt. **20,** 1361 (1981).
5. S. T. Chase and R. D. Joseph, "Resonant Array Bandpass Filters for the Far Infrared," Appl. Opt. **22,** 1775 (1983).
6. C. T. Cunningham, "Resonant Grids and Their Use in the Construction of Submillimetre Filters," Infrared Phys. **23,** 207 (1983).
7. R. Ulrich, "Far Infrared Properties of Metallic Mesh and Its Complementary Structure," Infrared Phys. **7,** 37 (1967).
8. R. Ulrich, "Effective Low-Pass Filters for Far Infrared Frequencies," Infrared Phys. **7,** 65 (1967).
9. G. Ragan, *Microwave Transmission Circuits,* MIT Radiation Laboratory Series (McGraw-Hill, New York, 1948), Vol. 9, p. 683.
10. M. S. Durschlag and T. A. DeTemple, "Far-IR Optical Properties of Freestanding and Dielectrically Backed Metal Meshes," Appl. Opt. **20,** 1245 (1981).
11. I. Anderson, "On the Theory of Self-Resonant Grids," Bell Syst. Tech. J. **54,** 1725 (1975).
12. N. Marcuvitz, *Waveguide Handbook,* MIT Radiation Laboratory Series (McGraw-Hill, New York, 1951), Vol. 10, pp. 280–285.
13. T. Timusk and P. L. Richards, "Near Millimeter Wave Bandpass Filters," Appl. Opt. **20,** 1355 (1981).
14. R. Compton, "Strip Gratings at a Dielectric Interface and Application of Babinet's Principle," preprint.
15. S. T. Shanahan and N. R. Heckenberg, "Transmission Line Model of Substrate Effects on Capacitive Mesh Couplers," Appl. Opt. **20,** 4019 (1981).
16. Shipley Co., Inc., 2300 Washington St., Newton, Mass. 02162.
17. Transene Co., Inc., Route 1, Rowley, Mass. 01969.
18. A. Lange, E. Kreysa, S. E. McBride, P. L. Richards, and E. E. Haller, "Improved Fabrication Techniques for Infrared Bolometers," Int. J. Infrared Millimeter Waves **4,** 689 (1983).
19. A. Lange and P. L. Richards, to be published.

Books *continued from page 1484*

Progress in Optics. Vol. 21. Edited by E. WOLF. North-Holland Publishing, New York, 1984. 446 pp. $67.25.

In the twenty-first volume of this series five excellent review articles have been written by leaders in their respective fields. To review these articles on a technical basis would require five different experts, and in a book review that is not feasible. Therefore, this is a short summary of the contents.

The first chapter by **D. Maystre** is a treatment of the rigorous vector theories of diffraction gratings. A brief historical introduction notes that the first attempt at solving the electromagnetic problem of gratings was made at the beginning of the century. Rayleigh based his approach on the assumption of the so-called Rayleigh hypothesis which assumes that the plane wave expansion remains valid inside the groove. The Rayleigh methods (and a similar approach due to Waterman) may be valuable in the study of some types of grating, it is concluded, but because of theoretical and numerical limitations these methods are far from being a near universal tool as are the integral methods which are discussed in detail. Differential and modal methods are also mentioned. The theory is applied to the case of metallic and dielectric gratings.

The theory of optical bistability is covered by **Luigi A. Lugiato.** After a historical introduction the semiclassical treatment is made of the steady-state behavior, transient behavior, instabilities in optical bistability, and the dressed-mode theory of optical bistability. The quantum statistical treatment considers the many-mode and one-mode master equation, the Fokker-Planck equation, and then, for transmitted light, the spectrum, the spectrum of fluorescent light, the photon statistics at steady state, and ends with the quantum mechanical treatment of transient behavior.

The Radon transform and its application are treated by **Harrison H. Barrett.** The Radon transform is relatively recent (1917) but has become of great importance in tomography as well as in x-ray crystallography, radio astronomy, electron microscopy, nuclear magnetic resonance, microwave scattering, and studies of the Fermi surface in metals. The 2-D Radon transform is considered first and then the 3-D case. The relationships to Abel, Cormack, Gegenbauer, and dipole-sheet transforms are given. There is also discussion of some varied applications of the Radon transform.

Zone plate coded imaging (ZPCI), and its theory and applications are considered by **Natale M. Ceglio** and **Donald W. Sweeney.** Simply, coded apertures are applied in a two-step process. In the first step, source information is recorded or encoded by geometrical shadow-casting through a coded aperture; in the second step, image reconstruction or decoding is achieved using a numerical or optical procedure matched to the coded aperture design. This review deals with apertures which are Fresnel zone plates. The impulse response analysis of the ZPCI is then given the eigenfunction analysis of continuous source distributions. A particular application of the method is made to laser fusion experiments.

Fluctuations, instabilities, and chaos in the laser-driven nonlinear ring cavity is the subject of the chapter by **John C. Englund, Robert R. Snapp,** and **William C. Schieve.** There is a nonlinearity which appears in the rate equations of spatially homogeneous systems and in the partial differential equations of systems with important spatial inhomogeneities. The ring cavity with a nonlinear medium as a mechanism for optical chaos is the case considered. The topics are the onset of instability, deterministic switching in the bistable regime, fluctuation dynamics, and the generation of deterministic chaos from instabilities.

The literature is cited in three of these reviews to 1983, one to 1982, and one to 1981. This volume has the same high quality as previous volumes of the series.

FRANKLIN S. HARRIS, JR.